Journal of Materials Chemistry A

Accepted Manuscript

ROYAL SOCIETY OF CHEMISTRY

www.rsc.org/materialsA

High energy density hybrid Mg^{2+}/Li^{+} battery with superior ultra-low temperature performance

Zhonghua Zhang,[1,2] Huimin Xu,[3] Zili Cui,[1] Pu Hu,[1] Jingchao Chai,[1] Huiping Du,[1] Jianjiang He,[1] Jianjun Zhang,[1] Xinhong Zhou,[3] Pengxian Han,[1] Guanglei Cui*[,1] & Liquan Chen[4]

[1]*Qingdao Industrial Energy Storage Research Institute, Qingdao Institute of Bioenergy and Bioprocess Technology, Chinese Academy of Sciences, Qingdao, 266101, P. R. China.*

[2]*University of Chinese Academy of Sciences, Beijing 100190, P.R. China.*

[3]*College of Chemistry and Molecular Engineering, Qingdao University of Science and Technology, Qingdao, 266042, P. R. China.*

[4]*Beijing National Laboratory for Condensed Matter Physics, Institute of Physics, Chinese Academy of Sciences, Beijing 102488, P.R. China.*

**Corresponding authors. Tel.: 86-532-80662746; fax: 86-532-80662746. E-mail: cuigl@qibebt.ac.cn*

Abstract

The development of high energy density rechargeable Mg-based batteries operated at wide electrochemical window and ultra-low temperature remains great challenge owing to parasitic side reactions between electrolytes and battery components when examined at high operating potential (above 2.0 V vs. Mg^{2+}/Mg). Herein we propose a flexible pyrolytic graphitic film (GF) as a reliable current collector of high-voltage cathode for hybrid Mg^{2+}/Li^{+} battery within a pouch cell configuration. The utilization of such a highly electrochemical stable GF unlocks the critical bottleneck of incompatibility among all battery parts, especially parasitic corrosive reactions between electrolyte and currently available current collector, which takes a big step forward towards Mg-based batteries' practical applications. With an operating potential of 2.4 V, our designed hybrid Mg^{2+}/Li^{+} battery can deliver a maximum energy density of 382.2 Wh kg^{-1}, which significantly surpasses that of the conventional Mg battery (about 60 Wh kg^{-1}), and the Al battery (about 40 Wh kg^{-1}) as well as the state-of-the-art hybrid Na/Mg and Li/Mg batteries. The electrochemical property of the hybrid Mg^{2+}/Li^{+} battery is also characterized by higher rate capability (68.8 mAh g^{-1} at 3.0 C), higher Coulombic efficiency of 99.5%, and better cyclic stability (98% capacity retention after 200 cycles at 1.0 C). In addition, the designed hybrid battery delivers excellent electrochemical performance at an ultra-low temperature of -40 ºC, at which it remains 77% capacity retention compared to that of room temperature. Our strategy opens up new possibility for widespread applications of graphitic current collectors towards high energy rechargeable Mg-based hybrid batteries, especially applied in polar regions, aerospace, and deep offshore waters.

1. Introduction

Owing to Mg anodes' low cost, dendrite-free and two-electron redox features, rechargeable Mg-based batteries are preferable for large-scale electrical energy storage, provided a host cathode and a compatible electrolyte can be explored that render the system with the necessary capacity, voltage, and cycle life at the prescribed charge/discharge rate.[1,2] However, the development of high performance rechargeable Mg battery is severely hindered by the limited choices of high energy density cathodes and the unavailability of well-matched electrolytes.[1–5] Hybrid batteries assembled by a Mg metal anode and a mature Li^+ ion intercalation cathode in mixed Mg^{2+}/Li^+ electrolyte are currently promising candidates for electrical storage systems, which address the above issues.[3,6–12]

Former hybrid Mg^{2+}/Li^+ batteries suffer from an unsatisfactory energy density due to the low intrinsic voltage of applied inorganic hosts (including Mo_6S_8,[3,10,12,13] TiS_2,[8,11] TiO_2[6] and $Li_4Ti_5O_{12}$[14]). Despite relatively high voltage cathodes, such as $LiFePO_4$ (LFP),[7,15] $MgCo_2O_4$,[9] $LiMn_2O_4$[16], have been proposed and tried to couple with Mg metals for hybrid Mg^{2+}/Li^+ batteries, their practical applications are technically unfeasible due to the limited anodic stability of the chosen electrolyte and the parasitic corrosive reactions between electrolyte and currently available non-noble metal current collector.[1,7,16] Wu et al. attempted to adopt a solid membrane (LISICON) to separate a Mg anode into a Grignard reagent-based organic electrolyte and a $LiFePO_4$ cathode into an aqueous lithium salt solution in an effort to realize a high operating potential and simultaneously avoid the parasitic corrosive reactions.[16] However, the poor electrochemical performance such as inferior coulombic efficiency and large over-potentials, along with the high cost and low conductivity of LISICON film dims their prospects towards practical application.

The major challenge for developing high voltage hybrid Mg^{2+}/Li^{+} batteries is to identify suitable electrolyte wherein Mg could be deposited reversibly whilst being compatible with all other battery components.[17–19] Grignard reagents, especially all phenyl complex (APC) type electrolyte, display 100% Mg deposition/stripping efficiency and highly anodic stability (~3.3 V) rendering them the currently most promising Mg battery electrolyte.[17] Notwithstanding optimal properties, the highly chlorinated Grignard reagent based electrolytes are severely corrosive to commonly available current collectors of rechargeable batteries, which results in a lower anodic electrochemical stability of the electrolytes below 2.0 V (vs. Mg^{2+}/Mg).[1] For example, Wang et al. revealed that the electrochemical corrosion of Cu current collectors occurred in the potential range of 1.80–2.40 V (vs. Mg^{2+}/Mg) in $Mg(AlCl_2EtBu)_2$/THF electrolyte.[18] Liu et al. identified that molybdenum and tungsten with highly electrochemical stability window (>2.8 V) could meet the rigid requirements of strong corrosive APC electrolyte by forming passive surface layers.[20] Nevertheless, the high cost constrained their large-scale application. Till now, choosing an affordable, electronically conducting and electrochemically inert current collector is still a major challenge in Mg rechargeable storage.

To evaluate the low temperature performance of any designed power device is vary valuable for many special applications, such as aerospace and military missions, which require batteries to be able to afford appropriate power capability and energy density at ultra-low temperatures (e.g. -40 ºC). Because of the solidification of carbonate-based electrolyte, conventional Li-ion technologies normally suffer from poor electrochemical performance when evaluated at -20 ºC or even lower temperature. Searching for energy storage devices with fair ultra-low temperature performance is still a major challenge until now.

Herein, we propose a facile and reliable strategy for high-voltage hybrid Mg^{2+}/Li^{+} battery by applying a flexible pyrolytic GF as a current collector for a commercial LFP cathode within a pouch cell configuration. In our proposed hybrid systems (Fig. 1), the Li^{+} ion intercalation/deintercalation occurs at the LFP cathode while the reversible Mg plating/stripping process takes place at the Mg anode. The working mechanism during discharge is shown as the following (Equation 1 to 3):

Cathode: $FePO_4+Li^{+}+e^{-}\rightarrow LiFePO_4$ Equation 1

Anode: $2Mg+3Cl^{-}+6THF\rightarrow[(\mu\text{-}Cl)_3Mg_2(THF)_6]^{+}+4e^{-}$ Equation 2

Full-cell: $4FePO_4+4Li^{+}+2Mg+3Cl^{-}+6THF\rightarrow 4LiFePO_4+[(\mu\text{-}Cl)_3Mg_2(THF)_6]^{+}$ Equation 3

Here, a well-known $[(\mu\text{-}Cl)_3Mg_2(THF)_6]^{+}$ dimer is identified as the formation targets of Mg dissolution reaction. Single-crystal X-ray diffraction analysis also has been carried out to identify the equilibrium species in the electrolyte solutions. As shown in Fig. S1, the solid state structure crystallizing from the THF solution of $PhMgCl\text{-}MgCl_2$ has been confirmed as an ionic pair $[Mg_2Cl_3(THF)_6]^{+}[AlCl_2Ph_2]^{-}$ product. It can be seen that the exact same cation is comprised of the three chloride bridged di-Mg core structure coordinated by three THF donors for each metal center, which has been presented in previous literatures[1,17,21]. This cation also has been widely accepted as the most important active species responsible for Mg plating/stripping cycles despite the fact that there exists other active species, demonstrated by Aurbach et al.[1,17] and Muldoon et al.[21].

Our facile strategy for realizing high-voltage hybrid Mg^{2+}/Li^{+} battery has several merits: 1) A GF current collector combined with pouch cell configuration not only preserves a wide electrochemical window of the APC-type electrolyte exceeding 2.8 V (vs. Mg^{2+}/Mg), but also

avoids the parasitic corrosive reactions between electrolytes and currently available current collectors; 2) Hybrid battery comprising of a LFP cathode and a Mg metal foil in mixed Mg^{2+}/Li^{+} electrolytes affords superior rate and cycling performance, meanwhile, delivers favorable features such as high operating potential (~2.45 V) and non-dendrite formation; 3) The hybrid battery with the tetrahydrofuran (THF)-containing electrolytes significantly outperforms their counterparts lithium ion batteries (LIBs) with carbonate-based electrolyte at the lower temperature of -20 and -40 ºC in virtue of the lower viscosity and melting points of THF-based solvents, which is preferable for many peculiar fields and places, such as polar regions, aerospace, and deep offshore waters; 4) Taking into account the abundant and environmentally friendly materials used in our systems, the designed hybrid Mg^{2+}/Li^{+} battery possesses superior advantages compared to other available rechargeable batteries in terms of cost, safety, and environmental considerations.

2. Experimental Section

2.1 Materials

Phenyl magnesium chloride (PhMgCl, Sigma-Aldrich Co. LLC., 2 M solution in THF); Anhydrous aluminum chloride ($AlCl_3$, Sigma-Aldrich Co. LLC., 99.999%); Anhydrous magnesium chloride ($MgCl_2$, Sigma-Aldrich Co. LLC., 99.99%); Anhydrous lithium chloride (LiCl, Sigma-Aldrich Co. LLC., 99.99%) Tetrahydrofuran (THF, Sinopharm group chemical reagent Beijing Co., Ltd); Magnesium metal foil (Mg, 99.999%); Stainless steel foil (SS, >99%); Nickel foil (Ni, >99%), Copper foil (Cu, >99%); Pyrolytic graphitic film (GF, Dupont Co., Ltd.); Lithium iron phosphate ($LiFePO_4$, Yantai zhuoneng battery material Co., Ltd.); Poly(vinyl difluoride) (PVDF); Acetylene black.

2.2 Preparation of electrolytes

2 M PhMgCl/THF solution and anhydrous $AlCl_3$ were used as received without further purification. The trace of water in THF was gotten rid of by reaction with sodium under refluxing. The electrolyte preparation was carried out under an argon atmosphere in a glove box containing less than 5 ppm water and O_2. The electrolyte, 0.5 M PhMgCl/$AlCl_3$ in THF, was prepared according to the previous literature.[10] In a typical procedure, 0.6666 g $AlCl_3$ was carefully added to 5 mL THF with vigorous stirring. Then, 5 mL of 2 M PhMgCl/THF solution was slowly added into the predetermined $AlCl_3$/THF solution with stirring for 24 h to form the APC electrolyte. The concentration of Li^+ ion varies from 0 to 0.4 M by adding different amounts of anhydrous LiCl in the electrolyte.

2.3 Characterizations

The morphology of each electrode (SS, Cu, Ni, GF and $LiFePO_4$@GF) surface before and/or after the electrochemical test were characterized using a field-emission scanning electron microscopy (FE-SEM, JSM 6700F). Energy dispersive spectrometry (EDS) was carried out on the same FE-SEM equipment to analyze the element distribution and composition of the various current collectors (both before and after the galvanostatic discharge-charge tests). The phase compositions of $LiFePO_4$@GF electrode were determined by X-ray diffraction (XRD, Rigaku D-max-γA with Cu K_α radiation). The crystallized product were isolated from the THF solution of PhMgCl-$MgCl_2$. It was washed with anhydrous THF before being transferred into an inert oil-sealed glass vial under argon. The single-crystal XRD measurement was carried out on the Bruker APEX-II CCD system. Data collection was performed at room-temperature with Mo-K_α, 0.71073 Å, radiation.

Crystal data for $C_{36}H_{58}AlCl_5Mg_2O_6$; Mr=839.67; Triclinic; space group P-1; a=12.959(3) Å; b=13.255(3) Å; c=13.746(3) Å; α=99.23(3)°; β=91.72(3)°; γ=104.14(3)°; V=2253.9(9) $Å^3$; Z=2;

T=293(2) K; λ(Mo-K_α)=0.71073 Å; μ(Mo-K_α)=0.459 mm^{-1}; dcalc=1.226 g cm^{-3}; 41,061 reflections collected; 8,557 unique (R_{int}=0.0362); giving R1=0.0613, wR2=0.1709 for 8557 data with [I>2σ(I)] and R1=0.0967, wR2=0.1947 for all data. Largest diff. peak/hole/e $Å^{-3}$: 0.70/-0.34.

2.4 Cell assembly and electrochemical measurements

All cell assembly processes were carried out in an argon-filled glove box with 0.1 ppm concentrations of both moisture and oxygen. For the fabrication of $LiFePO_4$@GF electrode, a mixture of commercial $LiFePO_4$, acetylene black, and PVDF at a weight ratio of 80:10:10 was pasted on GF. The electrode area was measured to be ~2 cm^2 and the mass loading of the active $LiFePO_4$ was calculated to be 1.5 mg cm^{-2} by weighting the mass variation of the loaded electrode and pure GF. Various current collectors (Cu, Ni, SS) and Mg metal anode were polished with sandpaper before used. Other LIBs cathodes are fabricated via the same procedure as that of the $LiFePO_4$@GF electrode.

The electrochemical properties of various current collectors (Cu, stainless steel, Ni and graphite film) were measured in three-electrode systems, in which a Mg foil was used as both counter electrode and reference electrode, and 0.25 M PhMgCl/$AlCl_3$ in THF solution was used the electrolyte, respectively. The scan potential was controlled from open circuit potential (OCP) to 3.2 V during Linear sweep voltammetry (LSV) analyses using electrochemical workstation (ZAHNER-Elektrik GmbH & Co. KG, Germany). Reversible Mg deposition/dissolution on graphite film was investigated by cyclic voltammetry (CV) between −1.0 V and 2.7 V at a scan rate of 5 mV s^{-1} using the same electrochemical workstation. The galvanostatic discharge-charge experiments were performed on a battery test system (LAND CT2001A,Wuhan Jinnuo Electronics., Ltd.) in order to calculate the Mg deposition/dissolution efficiency in CR2032 coin

cells. The galvanostatic discharge process was carried out at a current density of 0.2 mA cm^{-2} for 1 h, while the galvanostatic charge process was conducted to the cutoff potential of 2.5 V vs. Mg^{2+}/Mg. Electrochemical impedance spectroscopy (EIS) was conduct to investigate the effects of LiCl concentration in hybrid electrolytes on the kinetics of the LFP@GF electrode.

Pouch cells were assembled by using a $LiFePO_4$@GF electrode cathode and a Mg metal foil anode, which were separated by a layer of glass fiber filter paper. The mixed Mg^{2+}/Li^{+} electrolytes was injected and the cell was closed using a heat sealer to ensure air-tightness. The cell was removed from the glove box for long-term galvanostatic discharge-charge cycling stability tests (at 1 C, 1 C=170 mA g^{-1}) and rate capability experiments (e.g. 0.15, 0.3, 0.6, 1.2, and 3.0 C) within a potential between 2.1 and 2.8 V. The flexibility and durability of the LFP@GF electrode is evaluated via its electrochemical performance by CV (within a potential between 2.0 and 2.8 V at 1.0 mV s^{-1}) and EIS (with an amplitude of 10.0 mV and over a frequency range from 100 kHz to 100 mHz) measurements at flat and two bending states. CV curves at various scan rates were carried out to investigate the rate capability and kinetics of the cell reactions in three-electrode systems, in which a LFP@GF electrode was used as working electrode and two Mg foil was used as both counter electrode and reference electrode, respectively. The Li^{+} diffusion coefficient (D_{Li+}) can be calculated by applying the Randles-Sevcik equation: $I_p=2.69*10^5*n^{(3/2)}*A*D_{Li+}{}^{(1/2)}*C*\nu^{(1/2)}$, where I_p represents the peak current (A), n is the number of electrons per molecular reaction, A is the surface area of the cathode (cm^2), C is the lithium shuttle concentration (mol cm^{-3}), and ν is the scanning rate (V s^{-1}). The Nyquist plots of cells constructed from the various electrolyte-soaked separator and two stainless-steel plate electrodes, from which the ionic conductivities of electrolytes can be calculated via the equation: σ = L/(AR), where A and L are

the geometric area of the electrode and the thickness of the separator, respectively, and R represents the total resistance of the electrolyte. Taking the weights of all battery components into consideration, the accurate energy density is not easy to calculate. To facilitate comparison with previous reported results, we calculate the energy density only based on the total mass of the active cathodes as the following equation: E=C*V, in which E is energy density, C is the real discharge capacity of the applied electrode, and V is the operating voltage plateau at the applied current density. Galvanostatic discharge-charge cycling stability of the hybrid battery in a pouch cell and LIBs system in CR2032 coin cells are examined and compared at varied low temperature of 0, -10, -20, and -40 ºC at a current density of 170 mA g^{-1}.

3. Results and discussion

Firstly, we show Mg deposition/dissolution behavior when a flexible pyrolytic graphitic film is used as the working electrode in the APC electrolyte. Linear sweep voltammetry (LSV) experiments (Fig. 2a) have been performed in order to compare the anodic stability windows of the various current collectors including Cu, Ni, stainless steel (SS) and GF. For the Cu electrode, an apparent anodic current emerges at 1.8 V and continues to increase in the positive scan direction, probably caused by oxidation of Cu under high potential (>1.8 V).[18] Ni and SS electrodes deliver a relatively wide electrochemical window of 2.2 and 2.5 V compared to the Cu current collector, respectively. There is a direct comparison of their scanning electron microscopy (SEM) images and digital photos before and after galvanostatic discharge-charge experiments (See also Fig. S2, †ESI). The non-noble metals are oxidated into metal ions during charging and then diffuse to anode, followed by depositing on the Mg surface via direct replacement reactions demonstrated by the energy dispersive spectrometry (EDS) results (See also Fig. S3 for details,

†ESI). In contrast, the flexible GF electrode exhibits an enlarged electrochemical window exceeding 2.8 V (vs. Mg^{2+}/Mg), implying a much more anodic stability towards the electrolyte corrosion compared with traditional current collectors. Its excellent electrochemical corrosion resistance, especially in the APC electrolyte, may be ascribed to the entirely in-plane oriented graphitic structure with high crystallinity.[22–24]

The first three cyclic voltammetry (CV) cycles obtained from −1 V to 2.7 V using a GF working electrode and an APC electrolyte in three-electrode systems (Fig. 2b). The potential for the first Mg deposition and dissolution cycle is observed to be −0.48 and 0.13 V, respectively, and dropped to −0.39 and 0.08 V by the third cycle, respectively. Obviously, Mg deposition/dissolution process is highly reversible along with an almost 100% efficiency (See Tab. S1, †ESI). Figure 2c and 2d depict the typical galvanostatic charge and discharge profiles and the corresponding Mg dissolution/deposition efficiency for 50 cycles. The enlarged electrochemical window, almost 100% Mg dissolution/deposition efficiency and alleviated over-potentials demonstrated that graphite film was indeed a promising candidate as a cathode current collector for Mg-based batteries.

We then simply investigate the composition and morphology of the commercial LFP powder. All the X-ray diffraction peaks (Fig. 3a) can be well indexed to an orthorhombic olivine space group, pnma (ICDD PDF No. 40-1499), indicating a pure phase and highly crystalline LFP sample. SEM image of the LFP@GF electrode (Fig. 3b) depicts a rather rambling pattern comprising of microsized LFP particles and nanosized acetylene black particles. Photo images (inset of Fig. 3b) of both the LFP@GF electrode and pristine GF show that they possess flat surfaces without notable humps and cracks. In order to maintain a high coulombic efficiency, the cut-off voltage of

hybrid Mg^{2+}/Li^{+} battery is set at 2.8 V vs. Mg^{2+}/Mg, exceeding which significantly reduced efficiencies are detected (See also Fig. S4, †ESI), due to the severe electrolyte decomposition. Examined in a pouch cell configuration, the galvanostatic discharge-charge profiles of LFP@GF electrode (Fig. 3c) for hybrid Mg^{2+}/Li^{+} batteries display a very flat charge and discharge plateau ascribed to the redox reaction of Fe^{3+}/Fe^{2+}. It delivers a reversible discharge capacity of 103.7 mAh g^{-1} at 170 mA g^{-1}, which is much higher than previous reports.[7,16] The first five discharge curves are completely overlapped, indicating a superior reversibility of the LFP@GF electrode. The charge/discharge curves in Fig. 3c exhibit a lower voltage gap of 0.12 V compared with previous literature (0.8 V)[15], indicating a lower polarization degree of the LFP@GF electrode during the electrochemical reaction. More importantly, our hybrid Mg^{2+}/Li^{+} batteries exhibit excellent cycling performance (Fig. 3d). The initial capacity is 103.9 mAh g^{-1}, which decreases to 102.4 mAh g^{-1} after 200 cycles, with a good capacity retention of 98.5%. It should be noted that the coulombic efficiency of hybrid Mg^{2+}/Li^{+} batteries is maintained over 99.5% apart from the first several cycles.

No dendrite formation on the Mg anodes after galvanostatic discharge-charge tests at both 0.15 C and 3.0 C (See Fig. S5a and 5b, †ESI) was observed, which was significantly favorable to improve safety characteristic. Hybrid Mg^{2+}/Li^{+} battery delivers an initial reversible discharge capacity of 156.4 mAh g^{-1} at 0.15 C (Fig. 4a). A flat discharge plateau at the potential of 2.45 V may be ascribed to the potential difference between two phase reaction of $FePO_4/LiFePO_4$ and Mg dissolution reaction. The typical two-phase reaction mechanism of Li^{+} ion intercalation/deintercalation process is demonstrated by ex-situ XRD experiments (See Fig. S6, †ESI). As the charge-discharge rate increases from 0.3 C to 3.0 C, the discharge capacity of the

hybrid Mg^{2+}/Li^{+} battery is slightly decreased, and it delivers 144.1, 123.2, 96.6, and 68.8 mAh g^{-1} at a rate of 0.3, 0.6, 1.2, and 3.0 C, respectively, demonstrating a superior rate capability. It is found that the storage capacities are stable at each current rate (Fig. 4b). Moreover, the cell capacities can recover to the original value immediately when the current rate reverses back to 0.15 C. These results manifest that the hybrid Mg^{2+}/Li^{+} battery exhibits excellent cycling stability and rate capability.

CV curves of the LFP@GF electrode (Fig. 4c) are characterized by a pair of anodic and cathodic peaks ascribed to the redox reaction of Fe^{3+}/Fe^{2+}. Highly symmetric peak profiles are observed which signify good reversibility of both anodic and cathodic reactions. Besides, the peak current densities during anodic scans are in linear response to the square root of scanning rate (shown in Fig. 4d), indicating a typical diffusion controlled process. The lithium diffusion coefficiency (D_{Li+}) of the LFP@GF electrode is estimated to be 1.67×10^{-12} cm^2 s^{-1}, which is in agreement with that of previous report for lithium ion battery (the order arrange from 10^{-11} to 10^{-14} cm^2 s^{-1}).[25] The fast Li^{+} conductivity in the LFP cathode would favor high power applications. The capacity, rate performance and cycling stability are superior to the previously reported results of hybrid batteries (See Tab. S2 for details, †ESI) due to the non-occurrence corrosive reactions between electrolyte and current collector.[7,16]

We further investigate the effects of LiCl concentration in the hybrid electrolyte on the kinetics of the LFP@GF electrode via CV and electrochemical impedance spectroscopy (EIS) experiments (Fig. 5). Obviously, as the concentration of LiCl decreases, the lower peak current values and worse reproducibility of the sequent CV curves are observed (Fig. 5a and Fig. S7, †ESI), indicating that worse electrochemical kinetics are obtained from hybrid systems with lower LiCl

concentration. The CV curves overlap completely after the first five cycles in the 0.4 M LiCl and 0.5 M APC electrolyte (Fig. 5b), which demonstrates the highly reversibility of the LFP@GF electrode. In an effort to uncover the electrochemical kinetics derived from different LiCl concentrations, the interfacial resistances between Mg metal with varied electrolyte and the ionic conductivities of varied electrolyte have been characterized by the EIS tests (Fig. 5c). It could be found that the interfacial resistance was about 110, 55, 10, 8, and 3 KΩ for the hybrid electrolyte with 0, 0.01, 0.1, 0.2, and 0.4 M LiCl additives, respectively. The specific ionic conductivities (calculated from Nyquist plots in Fig. 5d) of the electrolytes with LiCl concentrations of 0, 0.01, 0.1, 0.2, and 0.4 M are estimated to be 1.03, 1.27, 1.35, 1.47, and 1.57 mS cm^{-1}, respectively. Given that the ionic conductivity of various electrolytes are similar, the improved electrochemical performance in a higher LiCl concentration electrolytes (i.e., 0.4 M LiCl) should be attributed to the significantly enhanced interfacial compatibility and/or the reduced interfacial resistance between Mg metal and the electrolyte.

There is an urgent task for developing power storage devices operated at extremely low environmental temperatures, especially below -20 ºC. These unique power suppliers would be a key requirement for many peculiar fields and places, such as polar regions, aerospace, and deep offshore waters, and so on. The low-temperature performance of the $LiFePO_4$@GF electrode was evaluated at the varied temperature of 0, -10, -20, and -40 ºC, compared with that of the commercial LIBs in which traditional carbonate-based electrolytes are used (shown in Fig. 6). The hybrid Mg^{2+}/Li^{+} battery and LIBs of the $LiFePO_4$@GF electrode delivers a high capacity of 103.5 and 109.8 mAh g^{-1} at a temperature of 0 ºC, respectively. The hybrid battery with the THF-containing electrolytes significantly outperforms their counterparts of LIBs with

carbonate-based electrolyte at the lower temperature of -20 ºC and -40 ºC in virtue of the lower viscosity and melting points of THF-based solvents applied in hybrid system, demonstrating its excellent low-temperature performance. An electric fan can be powered by two hybrid Mg^{2+}/Li^{+} pouch cell devices at the low temperatures (See also Fig. S8, †ESI). The above results further broaden the application markets of hybrid Mg^{2+}/Li^{+} battery to certain defense and space applications.

With an operating potential of 2.45 V, our designed hybrid Mg^{2+}/Li^{+} battery can deliver a maximum energy density of 382.2 Wh kg^{-1}, which significantly surpasses that of the state-of-the-art hybrid battery (Fig. 7). It is believed that, with optimal engineering, our designed hybrid system should potentially obtain high practical energy densities (due to the largely enhanced operating voltage), which is higher than that of the conventional Mg battery (about 60 Wh kg^{-1}),[5] and the Al battery (about 40 Wh kg^{-1})[26] as well as other previously explored hybrid Mg^{2+}/Li^{+} batteries.[3,6–16] In spite of the low-temperature durability and high energy density, our designed hybrid Mg^{2+}/Li^{+} battery also exhibits excellent flexibility and mechanical stability (See also Fig. S9 details, †ESI). Besides, we believe that our hybrid system can be promisingly expanded to various carbonaceous current collectors (such as flexible carbon clothes, carbon papers, graphene films, and so on), high voltage cathodes (such as $LiCoO_2$, and $LiFe_{0.2}Mn_{0.8}PO_4$), and newly explored electrolyte solutions (such as all inorganic magnesium aluminium chloride complex,[27] and magnesium borohydride,[28,29] and so on). Our work offers a facile and universal strategy to unlock the critical bottleneck of incompatibility among all battery parts on the way to Mg-based batteries' practical applications.

4. Conclusions

In summary, we presented an overall compatible hybrid Mg^{2+}/Li^{+} system with excellent electrochemical performance based on a flexible pyrolytic GF current collector, a relatively high-voltage $LiFePO_4$ cathode, a Mg metal anode and a mixed Mg^{2+}/Li^{+} electrolyte in a pouch cell configuration. Owing to the fully-compatible hybrid system, it operates at a high potential of 2.45 V and delivers a high specific capacity of 156.4 mAh g^{-1} at 0.15 C, a high rate capability (68.8 mAh g^{-1} at 3.0 C), and good cyclic stability (98% capacity retention after 200 cycles at 1.0 C). In addition, it exhibits excellent flexibility and superior low-temperature performance (77% capacity retention at -40 ºC) due to the utilized GF and low-melting point solvent, respectively. Considering low cost, dendrite-free, as well as excellent electrochemical performance of our designed hybrid system, we envision our universal and facile strategy opens up new possibility for widespread applications of promising graphitic current collectors and high-voltage cathodes for rechargeable Mg-based batteries with low-temperature and high potential durability.

Acknowledgements

This work was supported by the National High Technology Research and Development Program of China (863 Program, No. 2014AA052303-3), the National Natural Science Foundation of China program (No. 21271180) and the Key Technology Research Projects of Qingdao (No.13-CX-10).

References

1. S. Partha, K. D. Moni, I. V. Oleg, M. Ayyakkannu, A. David and N. K. Prashant, *Prog. Mater. Sci.*, 2014, **66**, 1–86.

2. H. D. Yoo, I. Shterenberg, Y. Gofer, G. Gershinsky, N. Pour and D. Aurbach, *Energy Environ. Sci.*, 2013, **6**, 2265–2279.

3. Y. Shao, T. Liu, G. Li, M. Gu, Z. Nie, M. Engelhard, J. Xiao, D. Lv, C. Wang, J. G. Zhang and J. Liu, *Sci. Rep.*, 2013, **3**, 3130.

4. M. Liu, Z. Rong, R. Malik, P. Canepa, A. Jain, G. Ceder and K. A. Persson, *Energy Environ. Sci.*, 2015, **8**, 964–974.

5. D. Aurbach, Z. Lu, A. Schechter, Y. Gofer, H. Gizbar, R. Turgeman, Y. Cohen, M. Moshkovich and E. Levi, *Nature*, 2000, **407**, 724–727.

6. S. Su, Z. Huang, Y. NuLi, F. Tuerxun, J. Yang and J. Wang, *Chem. Commun.*, 2015, **51**, 2641–2644.

7. S. Yagi, T. Ichitsubo, Y. Shirai, S. Yanai, T. Doi, K. Muraseb and E. Matsubar, *J. Mater. Chem. A*, 2014, **2**, 1144–1149.

8. H. D. Yoo, Y. Liang, Y. Li and Y. Yao, *ACS Appl. Mater. Interfaces*, 2015, **7**, 7001–7007.

9. E. Levi, Y. Gofer, Y. Vestfreed, E. Lancry and D. Aurbach, *Chem. Mater.*, 2002, **14**, 2767–2773.

10. Y. Cheng, Y. Shao, J. Zhang, V. L. Sprenkle, J. Liu and G. Li, *Chem. Commun.*, 2014, **50**, 9644–9646.

11. T. Gao, F. Han, Y. Zhu, L. Suo, C. Luo, K. Xu and C. Wang, *Adv. Energy Mater.*, 2014, **5**, 1401507.

12. J. Cho, M. Aykol, S. Kim, J. Ha, C. Wolverton, K. Y. Chung, K. Kim and B. Cho, *J. Am. Chem.*

Soc., 2014, **136**, 16116−16119.

13. Y. Gofer, O. Chusid, H. Gizbar, Y. Viestfrid, H. E. Gottlieb, V. Marks and D. Aurbach, *Electrochem. Solid-State Lett.*, 2006, **9**, A257–A260.

14. N. Wu, Z. Yang, H. Yao, Y. Yin, L. Gu and Y. Guo, *Angew. Chem. Int. Ed.*, 2015, **54**, 1−6.

15. Z. Chang, Y. Yang, X. Wang, M. Li, Z. Fu, Y. Wu and R. Holze, *Sci. Rep.*, 2015, **5**, 11931.

16. E. G. Nelson, S. I. Brody, J. W. Kampf and B. M. Bartlett, *J. Mater. Chem. A*, 2014, **2**, 18194–18198.

17. N. Pour, Y. Gofer, D. T. Major and D. Aurbach, *J. Am. Chem. Soc.*, 2011, **133**, 6270−6278.

18. D. Lv, T. Xu, P. Saha, M. K. Datta, M. L. Gordin, A. Manivannan, P. N. Kumta and D. Wang, *J. Electrochem. Soc.*, 2013, **160**, A351−A355.

19. S. Yagi, A. Tanaka, Y. Ichikawa, T. Ichitsubo and E. Matsubarab, *J. Electrochem. Soc.*, 2013, **160**, C83−C88.

20. Y. Cheng, T. Liu, Y. Shao, M. H. Engelhard, J. Liu and G. Li, *J. Mater. Chem. A*, 2014, **2**, 2473−2477.

21. H. S. Kim, T. S. Arthur, G. D. Allred, J. Zajicek, J. G. Newman, A. E. Rodnyansky, A. G. Oliver, W. C. Boggess and J. Muldoon, *Nat. Commun.*, 2011, **2**, 427.

22. P. Han, B. Zhang, C. Huang, L. Gu, H. Li and G. Cui, *Electrochem. Commun.*, 2014, **44**, 70−73.

23. M. T. Coltharp and N. Hackerman, *J. Phys. Chem.*, 1968, **72**, 1171−1177.

24. P. L. Antonucci, L. Pino, N. Giordano and G. Pinna, *Mater. Chem. Phys.*, 1989, **21**, 495−506.

25. K. Tang, X. Yu, J. Sun, H. Li and X. Huang, *Electrochim. Acta*, 2011, **56**, 4869−4875.

26. M. Lin, M. Gong, B. Lu, Y. Wu, D. Wang, M. Guan, M. Angell, C. Chen, J. Yang, B. Hwang

and H. Dai, *Nature*, 2015, **520**, 325−328.

27. R. E. Doe, R. Han, J. Hwang, A. Gmitter, J. I. Shterenberg, H. D. Yoo, N. Pour and D. Aurbach, *Chem. Commun.*, 2014, **50**, 243−245.

28. J. Muldoon, C. B. Bucur, A. G. Oliver, T. Sugimoto, M. Matsui, H. S. Kim, G. D. Allred, J. Zajicek and Y. Kotani, *Energy Environ. Sci.*, 2012, **5**, 5941−5950.

29. Y. Guo, F. Zhang, J. Yang, F. Wang, Y. NuLi and S. Hirano, *Energy Environ. Sci.*, 2012, **5**, 9100−9106.

Figure captions

Figure 1 Schematic illustration of the LFP|| hybrid electrolyte ||Mg battery during discharge.

Figure 2 (a) LSV curves of Cu, Ni, stainless steel and graphite film in the APC electrolyte from OCP to 3.2 V with a potential scan rate of 5 mV s^{-1}; (b) CV curves showing magnesium deposition/dissolution on a graphite film electrode in the APC electrolyte collected at a scan rate of 5 mV s^{-1} within the potential range from −1.0 to 2.7 V (vs. Mg^{2+}/Mg); The 1st, 2nd, 3rd, and 50th charge and discharge profiles (c) and the corresponding Mg dissolution/deposition efficiencies (d) of GF electrode.

Figure 3 (a) XRD pattern of the commercial LFP powders (inset: crystal structure of LFP); (b) Typical SEM image of the LFP@GF electrode (inset: photo images of LFP@GF electrode and pristine GF) ; (c) The first five galvanostatic discharge-charge profiles of LFP@GF electrode for hybrid Mg^{2+}/Li^{+} batteries in a pouch cell at 170 mA g^{-1}; (d) The discharge-charge cycling performance and the corresponding coulombic efficiency of the LFP@GF electrode for hybrid Mg^{2+}/Li^{+} batteries at room temperature.

Figure 4 Galvanostatic discharge-charge profiles (a) and the rate performance (b) of hybrid Mg^{2+}/Li^{+} batteries at varied rates; (c) CV curves of the hybrid Mg^{2+}/Li^{+} batteries at various scan rates in a three electrode cell; (d) The linear fitting of anodic peak current density vs. the square root of the scan rate. (1 C=170 mA g^{-1})

Figure 5 (a) CV curves of the hybrid Mg^{2+}/Li^{+} battery in the APC electrolyte with different amounts of LiCl at a scan rate of 1 mV s^{-1}; (b) The initial 10 cycles of CV profiles of the hybrid Mg^{2+}/Li^{+} battery in the APC electrolyte with 0.4 M LiCl; (c) Nyquist plots of Mg|| hybrid electrolyte ||Mg cells at room temperature; (d) Nyquist plots of cells constructed from the various

electrolyte-soaked separator and two stainless-steel plate electrodes.

Figure 6 Galvanostatic discharge-charge profiles (a and b) and cycling performance (c and d) of hybrid Mg^{2+}/Li^{+} battery (a and c) and traditional LIBs (b and d) at varied low temperatures.

Figure 7 Energy and power density comparison between our results and previously reported works.

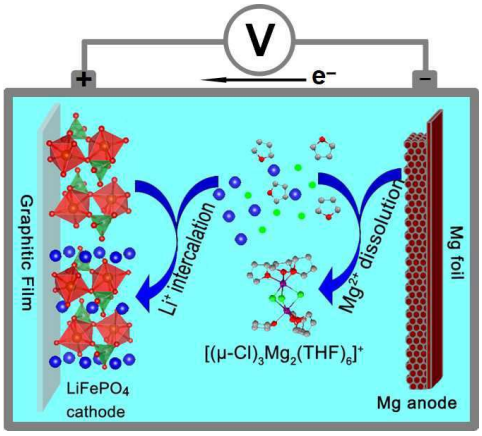

Figure 1

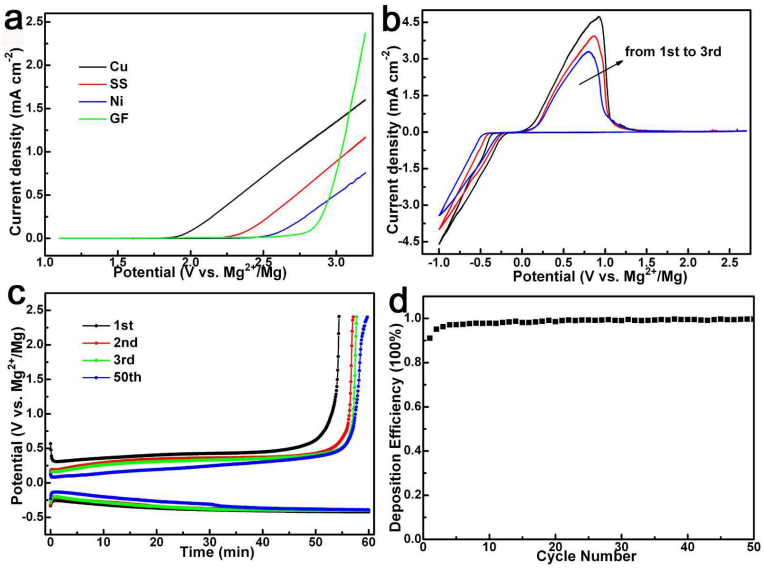

Figure 2

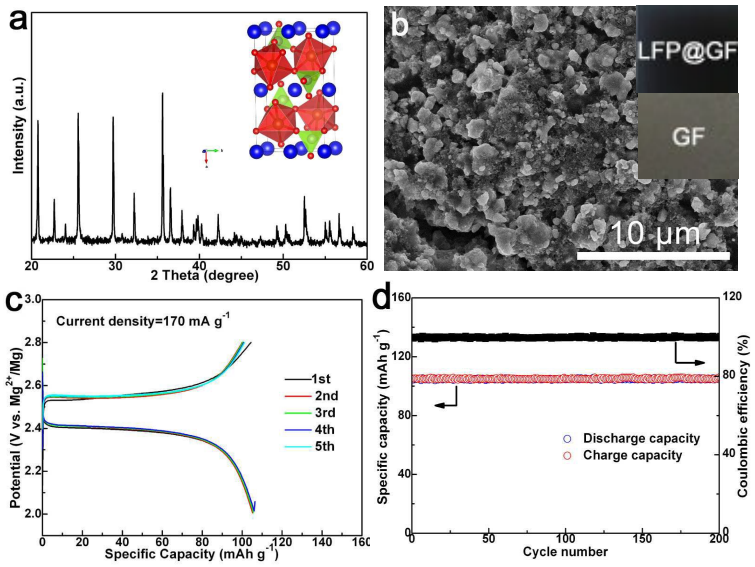

Figure 3

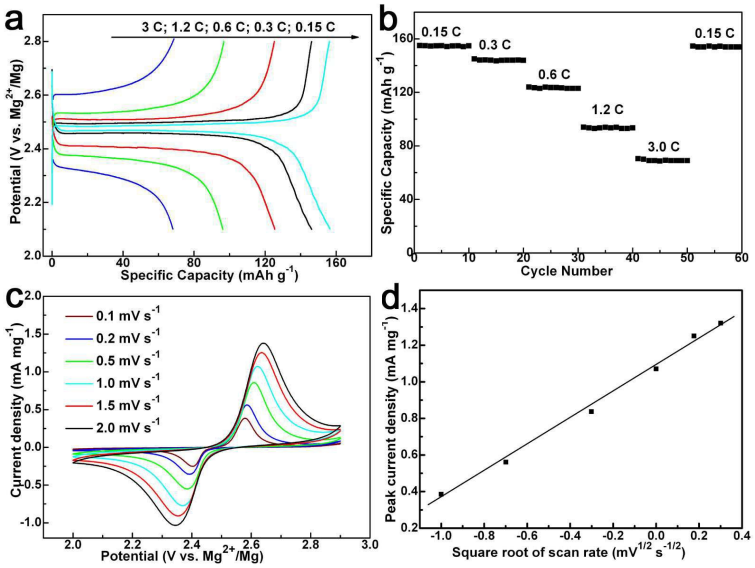

Figure 4

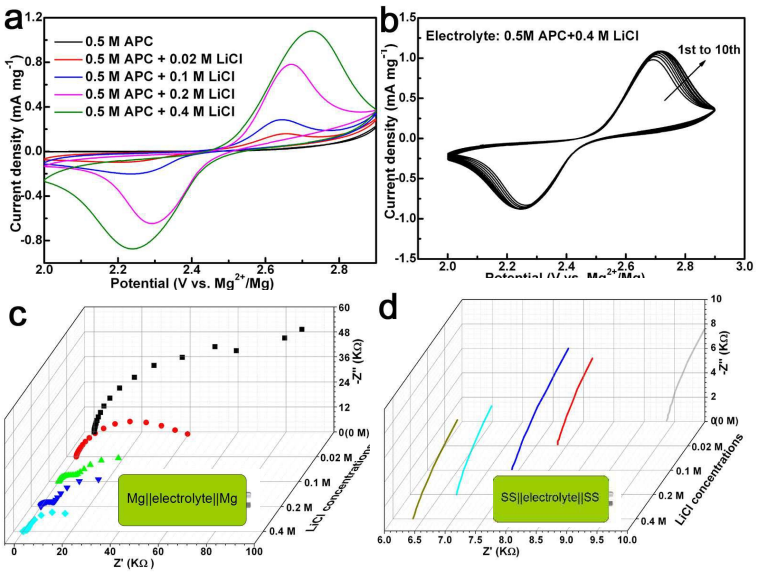

Figure 5

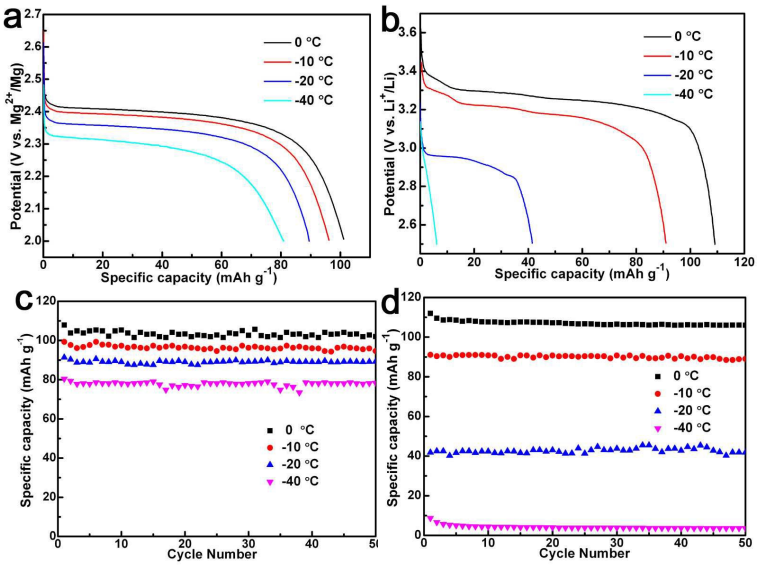

Figure 6

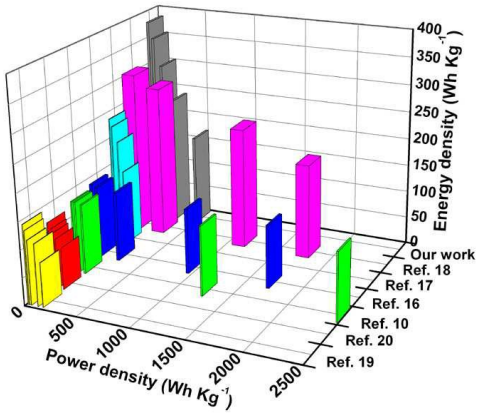

Figure 7